Since January 2020 Elsevier has created a COVID-19 resource centre with free information in English and Mandarin on the novel coronavirus COVID-19. The COVID-19 resource centre is hosted on Elsevier Connect, the company's public news and information website.

Elsevier hereby grants permission to make all its COVID-19-related research that is available on the COVID-19 resource centre - including this research content - immediately available in PubMed Central and other publicly funded repositories, such as the WHO COVID database with rights for unrestricted research re-use and analyses in any form or by any means with acknowledgement of the original source. These permissions are granted for free by Elsevier for as long as the COVID-19 resource centre remains active.

Bioelectrochemistry 146 (2022) 108106

Contents lists available at ScienceDirect

Bioelectrochemistry

journal homepage: www.journals.elsevier.com/bioelectrochemistry

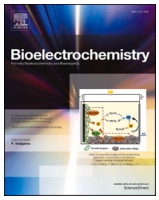

Label-free electrochemical aptasensor for rapid detection of SARS-CoV-2 spike glycoprotein based on the composite of $Cu(OH)_2$ nanorods arrays as a high-performance surface substrate

Zeinab Rahmati [a], Mahmoud Roushani [a,*], Hadi Hosseini [a], Hamzeh Choobin [b]

[a] Department of Chemistry, Faculty of Sciences, Ilam University, Ilam, P.O. BOX. 69315-516, Iran
[b] Department of Virology, Faculty of Medical Sciences, Tarbiat Modares University, Tehran, Iran

ARTICLE INFO

Keywords:
SARS-CoV-2
Aptamer-based sensors
Copper hydroxide nanorods
COVID-19
Spike glycoprotein

ABSTRACT

The development of advanced electrode materials and the combination of aptamer with them have improved dramatically the performance of aptasensors. Herein, a new architecture based on copper hydroxide nanorods ($Cu(OH)_2$ NRs) are directly grown on the surface of screen printed carbon electrode (SPCE) using a two-step in situ, very simple and fast strategy and was used as a high-performance substrate for immobilization of aptamer strings, as well as an electrochemical probe to development a label-free electrochemical aptasensor for SARS-CoV-2 spike glycoprotein measurement. The $Cu(OH)_2$ NRs was characterized using X-ray Diffraction (XRD) and electron microscopy (FESEM). In the presence of SARS-CoV-2 spike glycoprotein, a decrease in $Cu(OH)_2$ NRs-associated peak current was observed that can be owing to the target-aptamer complexes formation and thus blocking the electron transfer of $Cu(OH)_2$ NRs on the surface of electrode. This strategy exhibited wide dynamic range in of 0.1 fg mL^{-1} to 1.2 μg mL^{-1} and with a high sensitivity of 1974.43 μA mM^{-1} cm^{-2} and low detection limit of 0.03 ± 0.01 fg mL^{-1} of SARS-CoV-2 spike glycoprotein deprived of any cross-reactivity in the presence of possible interference species. In addition, the good reproducibility, repeatability, high stability and excellent feasibility in real samples of saliva and viral transport medium (VTM) were found from the provided aptasensor. Also, the aptasensor efficiency was evaluated by real samples of sick and healthy individuals and compared with the standard polymerase chain reaction (PCR) method and acceptable results were observed.

1. Introduction

Sensitive and selective designation of pathogens in complex actual samples is very significant. In global diseases for example coronavirus disease 2019 (COVID-19) pandemic, a selective, accurate, inexpensive, rapid and portable test is needed to diagnostic test at home and preventing the spread of the disease.

Recently, electrochemical sensors and biosensors have attracted a lot of attention due to their ability to detect selectively and sensitively a wide range of targets and in medical diagnosis and biomedical research, food control, environmental monitoring, forensics, drug discovery and etc. are of great importance [1–15]. Among the various biomolecules used to preparation of biosensing layers, aptamers have received much attention from researchers in recent years. Aptamers, as synthetic antibodies, are one of the most promising molecular probes that are synthesized and selected in vitro through the ligand evolution and also the exponential enrichment (SELEX) process and they can be used to detect a wide range of targets, from small molecules to intact cells [16–19]. Among the advantages of aptamers, which make them a noteworthy choice for the development of biosensors, are three-dimensional unique binding sites against their targets, low cost, easy modification, fast production, less immunogenicity, long-term stability, reversible denaturation and pH/temperature stability [20–27]. Different types of aptamer sensors (aptasensor) have been developed based on various transducers, including: electrochemical methods, surface plasmon resonance, colorimetric approach, fluorescence spectroscopy, optical transducers, etc. [28–32]. Among these techniques, electrochemical methods have received many attentions due to their innate high sensitivity, fast response times, real-time monitoring, simplicity, cost effectiveness, small sample amount requirement, low detection limits, amenability to miniaturization, etc. [33–36].

In recent years, with remarkable achievements in nanotechnology

* Corresponding author.
E-mail address: m.roushani@ilam.ac.ir (M. Roushani).

https://doi.org/10.1016/j.bioelechem.2022.108106
Received 18 November 2021; Received in revised form 19 March 2022; Accepted 21 March 2022
Available online 23 March 2022
1567-5394/© 2022 Elsevier B.V. All rights reserved.

and nanoscience and taking advantage of the attractive advantages of electrochemical methods and integration with bio-diagnostic elements as a receiver have received much attention for the production of sensitive and efficient biosensors. The use of nanostructures has been shown to have a significant effect on the performance of aptasensors. Proper nanomaterial design not only provides a good substrate for anchoring aptamer strings, but also dramatically increases the sensitivity and performance of aptasensors by creating a larger, more biocompatible surface [37–44]. For this purpose, various nanoparticles have been used to develop aptasensors, for example: quantum dots, metal nanoparticles, carbon-based nanostructures, conducting polymers metal organic frameworks, and so on [45–49]. Among these, nanoparticles based on transition metals are of great interest due to their mesoporosity, natural abundance, environmental friendliness, high electrocatalytic activity and high electrical conductivity [10,24,50,51].

Copper nanoparticles have been widely used owing to their distinctive properties including: availability, easy synthesis, cost-effective, low toxicity and biocompatibility [41,44,52,53]. Among the various methods of synthesizing copper nanoparticles, the in-situ growth method is an attractive method because nanoparticles can be synthesized directly on the surface of electrode without the need for adhesives and organic solvents, which is fast and facile synthesis procedure and has the ability to morphological controllability and thickness. Also, in comparison with traditional methods of electrode modification, such as drop or film casting, this method prevents the aggregation of nanoparticles and is uniformly placed on the electrode surface, leading to increased stability, conductivity and their active surface [54–55]. Cu $(OH)_2$ NRs, in addition to providing an extremely large surface area for aptamer strings further loading, also act as a suitable electroactive substrate owing to the large amount of copper placed on the electrode surface and the creation of an excellent cathodic current in the phosphate buffer, therefore, it can be a unique choice as a platform for the preparation of label free and ultrasensitive electrochemical aptasensors. $Cu(OH)_2$ NRs have shown significant performance in a variety of applications including electrocatalysis, and energy storage because of their good electrocatalytic performance and high surface area but as far as we know, they have not yet been used to improve the performance of electrochemical biosensors [54–58].

In this study, a new architecture is designed to increase the efficiency of label free and ultrasensitive electrochemical aptasensor based on Cu $(OH)_2$ NRs to SARS-CoV-2 spike glycoprotein measurement. $Cu(OH)_2$ NRs are directly synthesized on the SPCE surface using a two-step in situ, very simple and fast method. The provided aptasensor showed satisfactory results in the diagnosis of SARS-CoV-2 spike glycoprotein including a wide dynamic range, low detection limit, selectivity and possibility of application in real samples. Also, compared to the PCR test of real samples of sick and healthy individuals, the results were very promising.

2. Experimental section

2.1. Materials

SARS-CoV-2 spike glycoprotein was purchased from cusabio Company (https://www.cusabio.com). The sequence of specific aptamer for SARS-CoV-2 spike glycoprotein [59] that was purchased from Bioneer Company (South Korea) is indicated below: 5′-NH_2-TCGCTCTTTCCGCTTCTTCGCGGTCATTGTGCATCCTGACTGACCC-TAAGGTGCGAACATCGCCCGCGTAAGTCCGTGTGTGCGAA-3′.

Analytical grade of sodium hydroxide (NaOH >99%), ammonium proxydisulfate ($(NH_4)_2S_2O_8$ >98%), copper sulfate ($CuSO_4$ >99%), ammonium sulfate ($(NH_4)_2SO_4$ >99.5%) and all other reagents were bought from Merck or Sigma-Aldrich and they were used without additional purification. Furthermore, 0.1 M disodium hydrogen phosphate (Na_2HPO_4 >99%) and monosodium dihydrogen phosphate (NaH_2PO_4 >99%) were used to preparing the phosphate-buffered solutions (PBS). The all experiments were performed at room temperature.

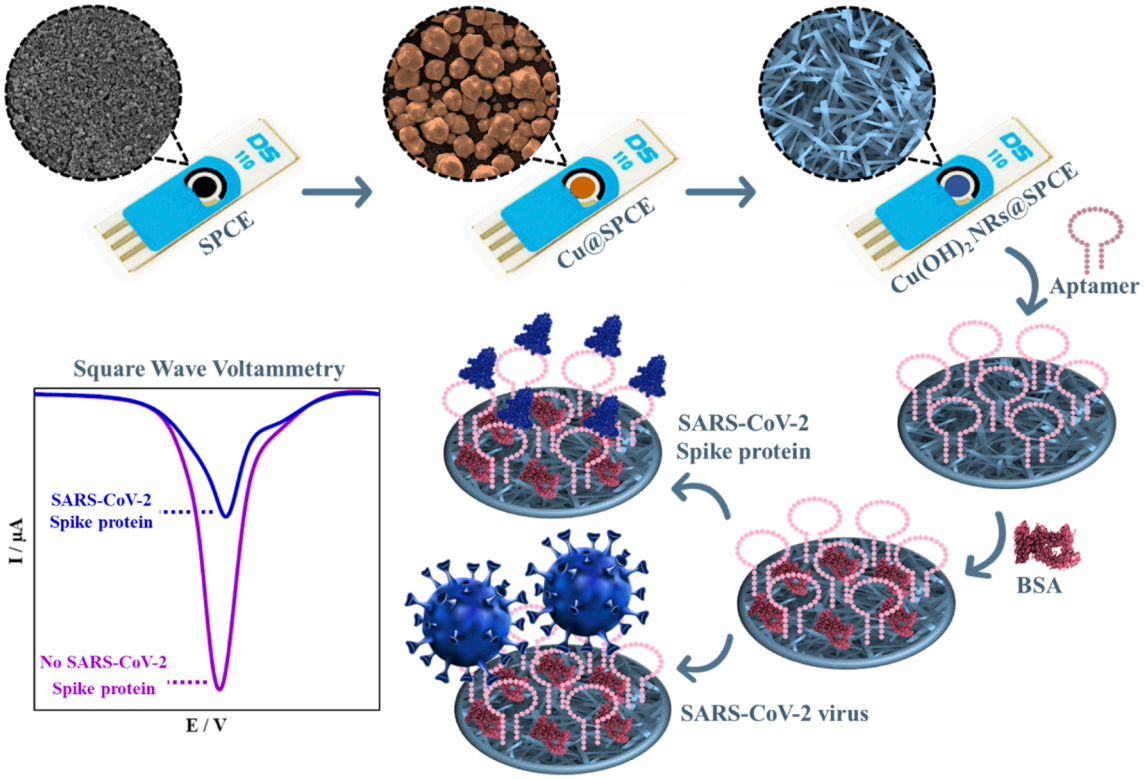

Scheme 1. Schematic illustration of the steps of the aptasensor preparation.

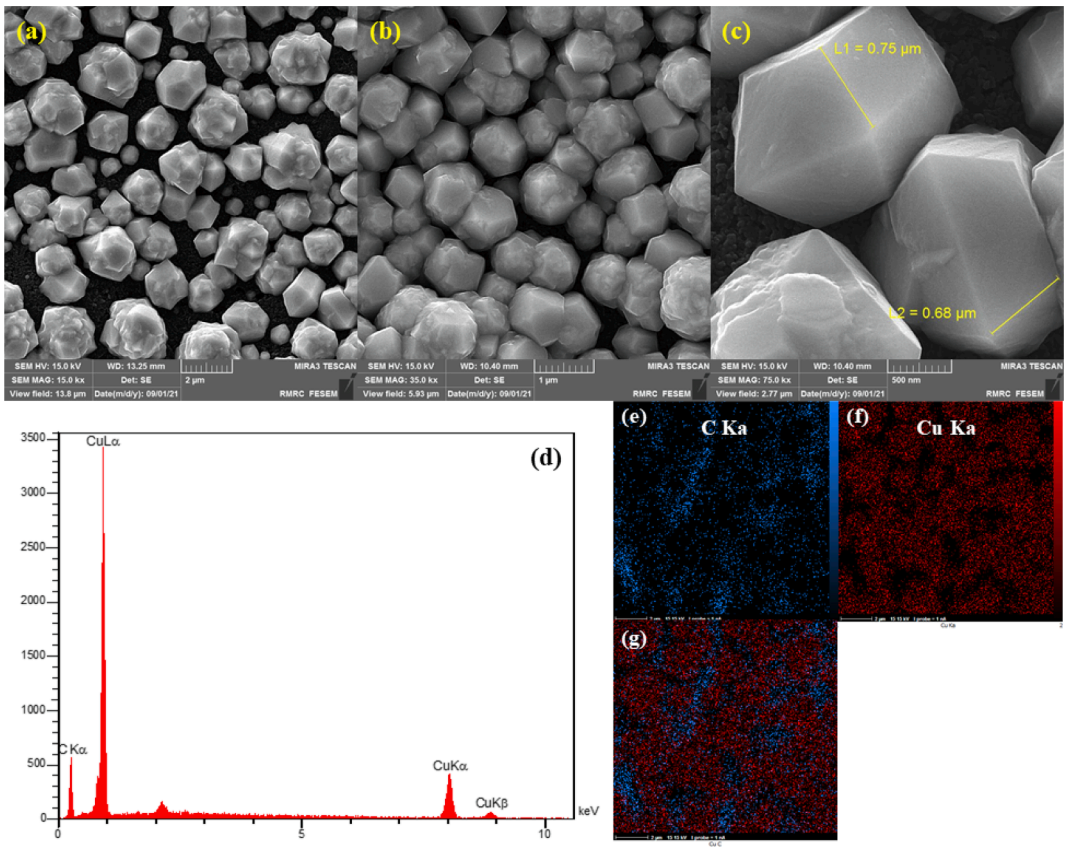

Fig. 1. The FESEM images of Cu@SPCE (a-c), EDX spectrum (d) and EDS mapping of Cu@SPCE (e-g).

2.2. Instruments and electrodes

In order to investigate surface morphology, a MIRA3 TESCAN-LMU field-emission scanning electron microscope (FESEM) was applied which was then equipped with an EDS probe. The electrochemical investigations were recorded using a μ-Autolab type III/FRA2 (Eco Chemie B.V., Ultrecht, The Netherlands) instrument equipped with NOVA software. The SPCE (bought from Dropsens (Spain)) was applied as a three-electrodes planar based on a graphite working electrode, silver pseudo-reference electrode and a carbon counter electrode. In order to measure the pH, the Metrohm pH meter (model 780 pH/mV meters) was applied.

2.3. Cu@SPCE fabrication

The Cu@SPCE and $Cu(OH)_2$ NRs@SPCE were prepared following the previous literature reports [55]. Before modification of SPCE, its surface was cleaned by electrochemical method. For this purpose, 10 μL of NaOH solution (0.1 M) was dropped onto the surface of SPCE and a sweeping potential was applied during 10 consecutive cycles and finally, the electrode was dried under N_2 gas. Then, 10 μL of the 0.5 M of $(NH_4)_2SO_4$ solution containing 0.02 M of $CuSO_4$ was dropped on the surface of electrode and a constant potential of − 0.6 V during 600 s was applied in order to the electro-deposition of Cu clusters with suitable thickness and brilliant rose gold-colored onto SPCE surface (Cu@SPCE).

2.4. $Cu(OH)_2$ NRs@SPCE fabrication

In order to in situ growth the $Cu(OH)_2$ NRs on the surface of SPCE a drop of an alkaline oxidant solution containing 3.0 mL of DI water, 0.7 mL of $(NH_4)_2S_2O_8$ (1 M) and 1.4 mL of NaOH (10 M) it was placed on the electrode at room temperature. After 2 min, the Cu metal film turned into a uniform blue-colored $Cu(OH)_2$ NRs [55,56]. Then, $Cu(OH)_2$ NRs@SPCE was washed with DI water and dried under N_2 gas. $Cu(OH)_2$ NRs@SPCE was used in order to develop of label free and ultrasensitive electrochemical aptasensor.

2.5. Preparation of the aptasensor

In this step, a drop of 5′-NH_2-aptamer solution (3 μM) was dropped on the $Cu(OH)_2$ NRs@SPCE surface for 1 h to immobilize the aptamer strings. Next, aiming at block the available non-bonded active surface, and avoid nonspecific adsorption, the BSA solution (10 μL of 1%) was incubated on the aptamer/$Cu(OH)_2$ NRs@SPCE surface for 30 min. Also, if not used of BSA, many non-specific sites cause non-specific adsorption, and results obtained from the measurements will not be accurate, because in real samples, other components of the real samples may cause interference in the signal peak due to blockage of other proteins, presence of ions, etc. The resulting electrode was named BSA/aptamer/Cu$(OH)_2$ NRs@SPCE in this step. After each step, DI water were used to wash the electrode surface to remove the unbonded molecules and dried under N_2 gas.

3. Results and discussion

3.1. Investigation of the $Cu(OH)_2$ NRs/SPCE characterization

The electrode modification method by $Cu(OH)_2$ NRs is shown in Scheme 1. The following mechanism that proposed by Zhang et al., can be explained the fabrication of.

$Cu(OH)_2$ NRs [60]:

$$Cu + 4NaOH + (NH_4)_2S_2O_8 \rightarrow Cu(OH)_2 + 2Na_2SO_4 + 2NH_3\uparrow + 2H_2O \quad (1)$$

In alkaline solution, the surface of metallic copper was quickly converted and oxidized to Cu^{2+} using $(NH_4)_2S_2O_8$ after only a few

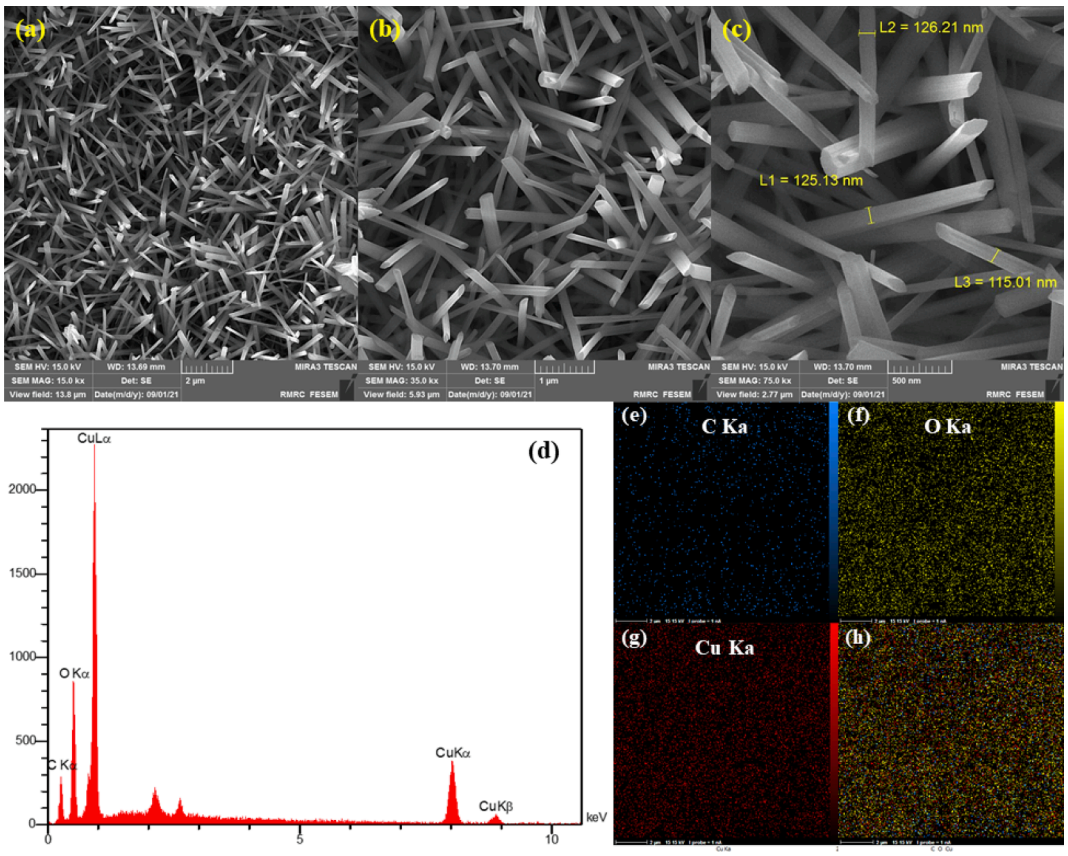

Fig. 2. The FESEM images of $Cu(OH)_2$ NRs@SPCE (a-c), EDX spectrum (d) and EDS mapping of $Cu(OH)_2$ NRs@SPCE (e-h).

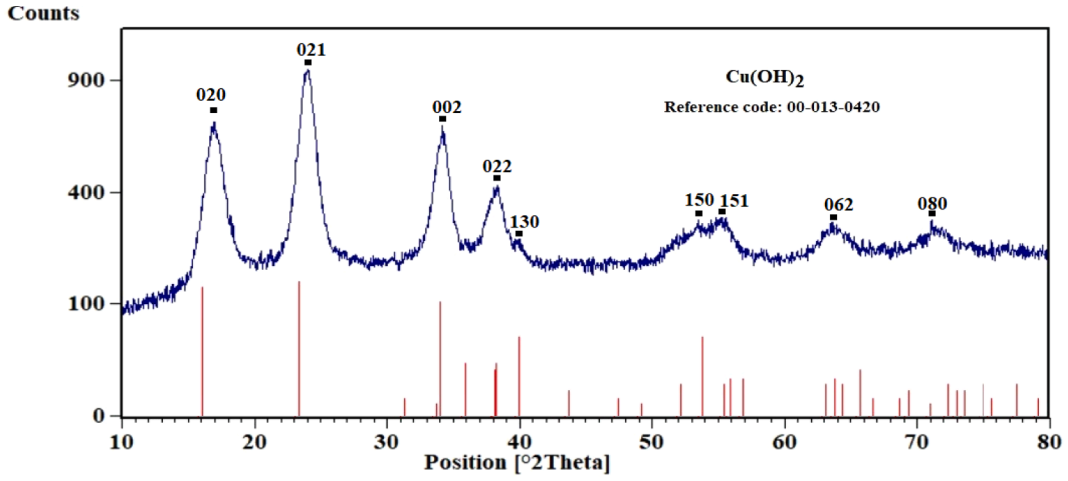

Fig. 3. The XRD patterns of as-prepared $Cu(OH)_2$ NRs.

minutes. Then, due to the highly alkaline condition, square planar coordination of Cu^{2+} to OH^{-1} groups was occurred, giving rise to stoichiometric chains alone. Then, these chains were connected through the bridging OH^{-1} groups along the z-axis, which formed a nanowires structures [60].

In order to monitoring the structure and morphology of rod-like structures of $Cu(OH)_2$ NRs/SPCE, the FESEM images were used. Initially, the morphology of metallic copper that deposited on the surface of SPCE was investigated. As shown in Fig. 1a–c, the well-ordered and vertically Cu clusters arrays, which are made from the accumulation small particles of its, were uniformly deposited on the SPCE surface which provides surface availability for the formation of $Cu(OH)_2$ NRs structures. Next, the Cu clusters were converted to $Cu(OH)_2$ NRs via chemical oxidation technique and the surface morphology of the blue film formed on the electrode surface was investigated using FESEM images. The FESEM images in Fig. 2a–c display the morphology changes of Cu clusters during the process of chemical conversion to $Cu(OH)_2$ NRs by diameter of 100 nm, which grown in different directions and uniformly cover the surface of the electrode.

The EDX results were examined to evaluate elemental composition of the modified SPCE at each stage. Fig. 1d shows the EDX spectrum of Cu@SPCE, which shows the attendance of Cu in Cu@SPCE, C that originated from SPCE. Moreover, in the $Cu(OH)_2$ NRs @SPCE EDX spectrum, in addition to the elements Cu and C, O was observed, which

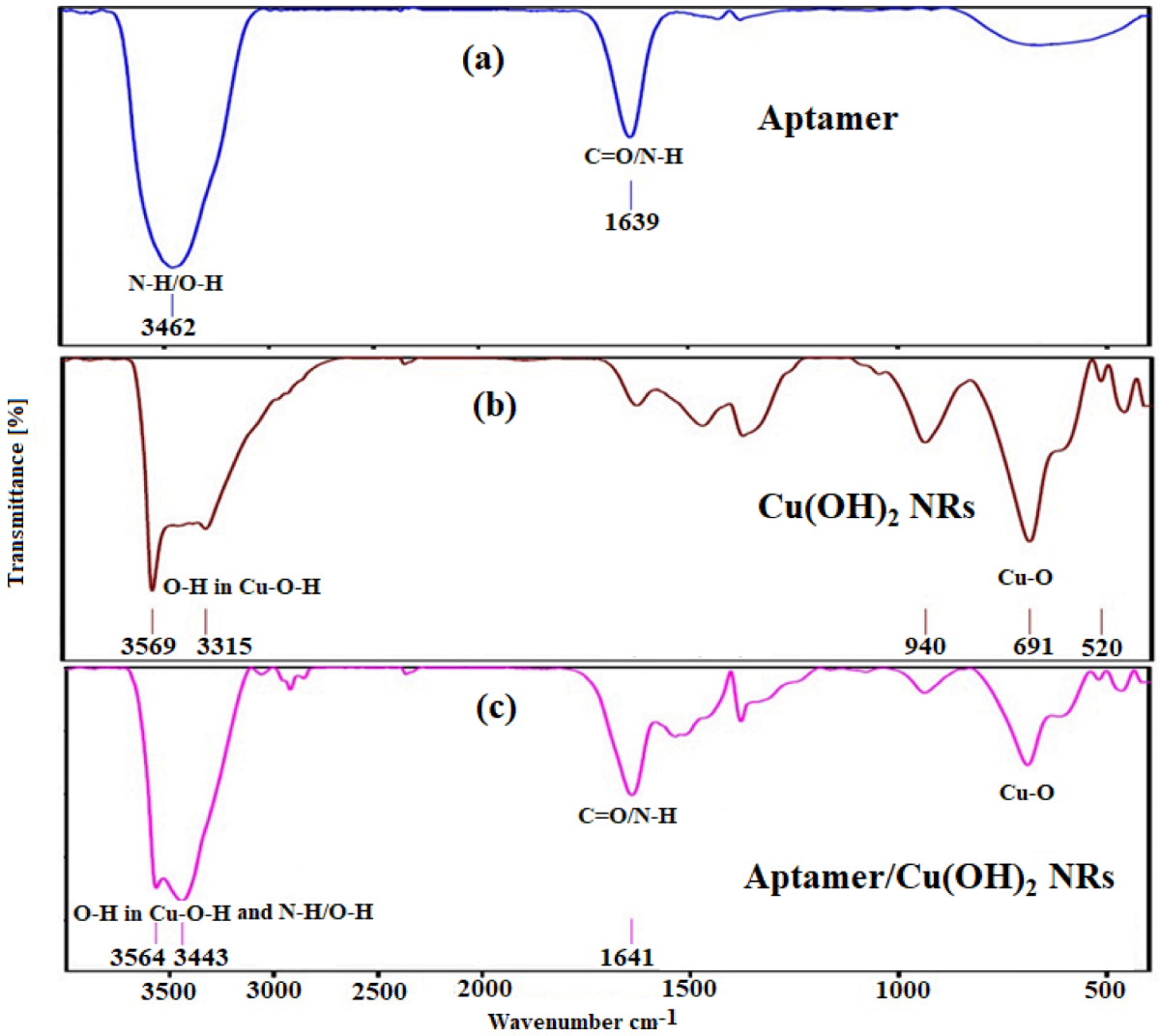

Fig. 4. The FTIR spectrums of (a) aptamer, (b) as-prepared $Cu(OH)_2$ NRs, and (c) aptamer/$Cu(OH)_2$ NRs.

confirms the successful change of Cu to $Cu(OH)_2$ NRs (Fig. 2d). Furthermore, the EDS mapping displaying the well and uniform distribution of Cu clusters on the Cu@SPCE (Fig. 1e-g) and Cu and O for Cu $(OH)_2$ NRs@SPCE (Fig. 2e-h) (C originated from SPCE). These results were consistent with the literature [55,56].

In order to evaluate the crystal structure of the as-prepared $Cu(OH)_2$ NRs, the XRD technique was applied (Fig. 3). The $Cu(OH)_2$ NRs shows diffraction peaks at 16.7, 23.8, 34.0, 38.2, 39.8, 53.2, 56.2, 63.4, 71.1° that are well matched with the (020), (021), (002), (022), (130), (150), (151), (062), (080) planes of the standard crystallographic spectrum of Orthorhombic $Cu(OH)_2$ (JCPDS no. 013-0420) structure with standard lattice constants of $a = 2.949$ Å, $b = 10.590$, $c = 5.256$ Å (Fig. 3), confirming the successful preparation of pure $Cu(OH)_2$ NRs.

The FT-IR spectroscopy was further applied to study the structure of $Cu(OH)_2$ NRs and also the interaction of aptamer with $Cu(OH)_2$ NRs. Fig. 4a shows the FTIR spectrum of aptamer with two sharp peaks at 3462 and 1639 cm^{-1}, which can be related to the N—H/O—H and C═O/N—H vibrations modes in the aptamer strings, respectively. The FT-IR spectrum of the synthesized $Cu(OH)_2$ NRs shows two strong peaks at 3569 and 3315 cm^{-1} related to the O—H stretching vibration mode in Cu—O—H structure which supports the formation of hydroxyl groups at Cu $(OH)_2$ NRs, and the peaks at 940, 691, and 520 cm^{-1} can be related to the Cu—O stretching and Cu—O—H bending vibrations modes (Fig. 4b) [55,61]. Moreover, the band around 1374–1628 cm^{-1} shows the stretching mode of the absorbed water in the $Cu(OH)_2$ NRs. The FTIR spectra of aptamer/$Cu(OH)_2$ NRs shows some differences compared to the $Cu(OH)_2$ NRs (Fig. 4c). Change in the position and the intensity of O—H/N—H group in 3443 cm^{-1} and the appearance of C═O group in 1641 cm^{-1} can be indicated a successful attachment of the aptamer onto the $Cu(OH)_2$ NRs.

3.2. *Electrochemical study of the proposed aptasensor stepwise preparation*

The step-by-step fabrication process of aptasensor was characterized by square wave voltammetry (SWV) in BPS (0.1 M) with pH 7.4 (Fig. 5A). First, for the bare SPCE no obvious peak was observed (curve a, $I_{pc} = 0$). After $Cu(OH)_2$ NRs was embellished on SPCE surface (curve b, $I_{pc} = -152.87$), an cathodic peak current of $Cu(OH)_2$ NRs at −0.17 V was clearly appeared that this cathodic peak is suspected to be due to the electroreduction of $Cu(OH)_2$ to Cu_2O [62,63]. In the next step, as expected, after the immobilization of the aptamer strings as non-electroactive substance, the peak current reduced significantly (curve c, $I_{pc} = -101.32$), because the aptamer strings hindered electron transfer due to steric/conformational restrictions. After this step, similarly, cathodic peak current was further reduced with BSA assembled on the surface of modified electrode (curve d, $I_{pc} = -83.33$), indicating blockage of possible residual active site at the surface of modified electrode, however, good electrochemical activity was still observed from the modified electrode. Interestingly, after the embellishment of

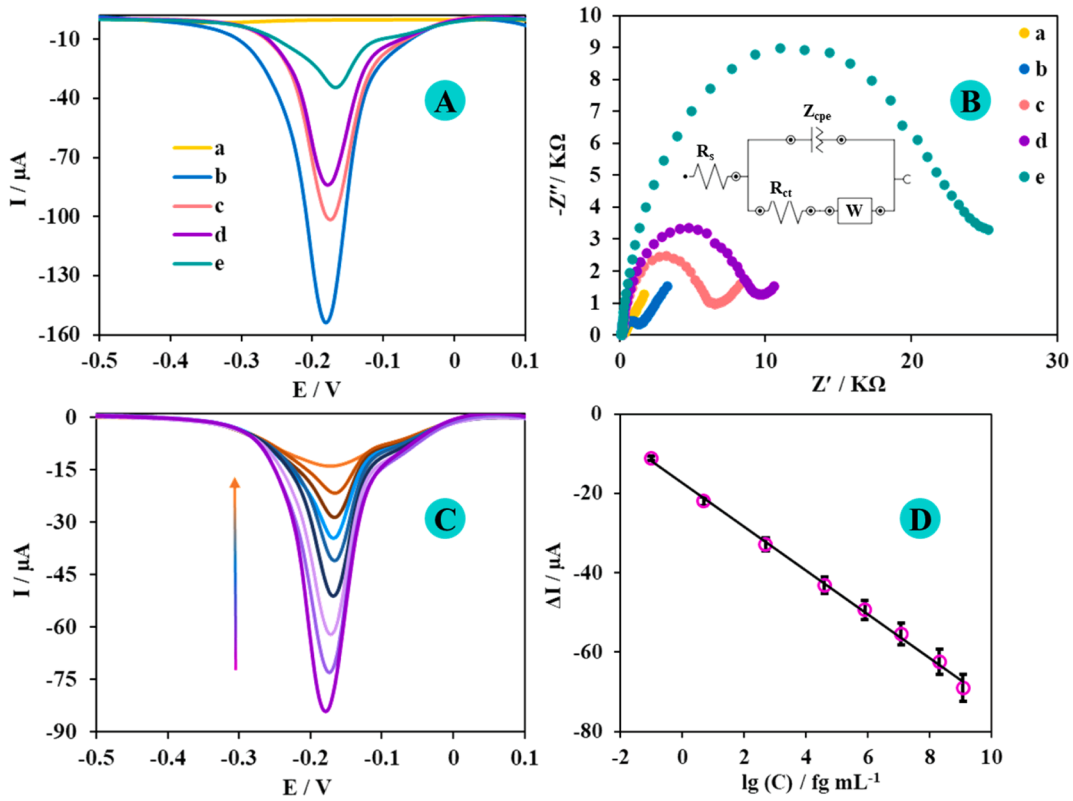

Fig. 5. (A) SWV characterization of different modified electrodes in PBS with pH = 7.4 and (B) EIS characterization in PBS with pH = 7.4 containing $K_3Fe(CN)_6$/ $K_4Fe(CN)_6$ (5 mM) in a 1 to 1 ratio: (a) SPCE, (b) $Cu(OH)_2$ NRs@SPCE, (c) Apt/$Cu(OH)_2$ NRs@SPCE, (d) BSA/Apt/$Cu(OH)_2$ NRs@SPCE and (e) SARS-CoV-2 spike glycoprotein/BSA/Apt/ $Cu(OH)_2$ NRs@SPCE, inset B: the obtained equivalent circuit. (C) The SWV response of the provided aptasensor after incubating with different concentrations of the SARS-CoV-2 spike glycoprotein solutions in range of 0.1 fg mL^{-1} to 1.2 µg mL^{-1} (n = 3) in PBS with pH = 7.4. (D) Calibration curve of $Cu(OH)_2$ NRs-associated cathodic peak current of related to aptasensor vs log $C_{\text{SARS-CoV-2 spike glycoprotein}}$ (fg mL^{-1}). The regression equation was ΔI (µA) = −5.5284 log C (fg mL^{-1}) − 17.319 (R^2 = 0.9979).

800 pg mL^{-1} of the SARS-CoV-2 spike glycoprotein, cathodic peak current reduced obviously (curve e, I_{pc} = −34.66), shows that aptamer strings have captured the target molecules and the formation of SARS-CoV-2 spike glycoprotein-aptamer complex, induced conformational changes of the bound aptamers and increase steric/conformational restrictions that increased the space barrier and retard the electrolyte solution to reach the SPCE surface. These observations showed that the aptasensor preparation was successful.

Further, the electrochemical behaviors each step of electrode modification were investigated using electrochemical impedance spectroscopy (EIS) responses, as a sensitive electrochemical technique [7], in PBS with pH = 7.4 containing $K_3Fe(CN)_6$/ $K_4Fe(CN)_6$ (5 mM) in a 1 to 1 ratio at a potential of 0.23 V. Fig. 5B displays the Nyquist plots that the observed semicircle portion at high frequencies is associated the electron-transfer resistance (R_{ct}) and the linear part at low frequencies is associated the finite propagation process. First, a quite small resistance to electron-transfer was observed for the bare SPCE (R_{ct} = 0.31 kΩ, curve "a"). The diameter of semicircle increased after $Cu(OH)_2$ NRs was embellished on SPCE surface (R_{ct} = 1.4 kΩ, curve "b"), due to the repulsion force between the $Cu(OH)_2$ NRs, which has a negative charge and the anionic redox probe species that lead to increased R_{ct}. As expected, R_{ct} increased significantly after immobilization of the aptamer strings on the modified SPCE surface, due to the creation of a steric hindrance at the electrode surface (R_{ct} = 6.54 kΩ, curve "c"). Similarly, regarding the incubation of BSA at the surface, the R_{ct} increased (R_{ct} = 8.7 kΩ, curve "d") and when incubating with 800 pg mL^{-1} of the SARS-CoV-2 spike glycoprotein, R_{ct} increased obviously (R_{ct} = 24.9 kΩ, curve "e"), representing a successful connection of SARS-CoV-2 spike glycoprotein to aptamer strings. Thereby, the EIS signals which were consistent with SWV response confirm the correctness of the aptasensor development. Besides, inset Fig. 5B showed a Randles equivalent circuit was well-fitted with the obtained plot and the symbols in the equivalent circuit include the solution resistance (R_s), the constant phase element (Z_{cpe}), the Warburg impedance element (Z_W) and the resistance of the charge-transfer (R_{ct}). A comparison between experimental impedance data with the data obtained by nonlinear fitting using the Randles equivalent circuit for the aptasensor showed this data fits well in this circuit equivalent. The most important parameter in this study is R_{ct}, which indicates the resistance to charge transfer between the redox probe and the surface of electrode. Therefore, to estimate the R_{ct}, all EIS experimental data were fitted in equivalent circuits. The circuit fitting data with fitting percentage are shown in Fig. S1.

3.3. Optimization study of the experiment

Some parameters need to be optimized to achieve the best sensing performance of aptasensor. Optimal aptasensor preparation conditions were evaluated by SWV response in PBS with pH = 7.4. A neutral medium is obligatory to avoid the being demolished of aptamer strings as biological molecules, so all experiments are carried out in PBS at pH 7.4. The concentration and time required for immobilization of aptamer were optimized as important factors in preparation of aptasensors. Therefore, the aptamer concentration on the surface of electrode could directly affect the target capture efficiency. As displayed in the Fig. S2A and B, the most adsorption of aptamer strings on the surface of the modified electrode was 3 µM and the incubation time was selected as 1 h. If there is not enough time to immobilize the BSA molecules, many non-specific sites cause non-specific adsorption, so, we optimized the incubation time of BSA as significant parameter and 30 min was chosen as the optimum incubation time (Fig. S2C). Furthermore, to get the

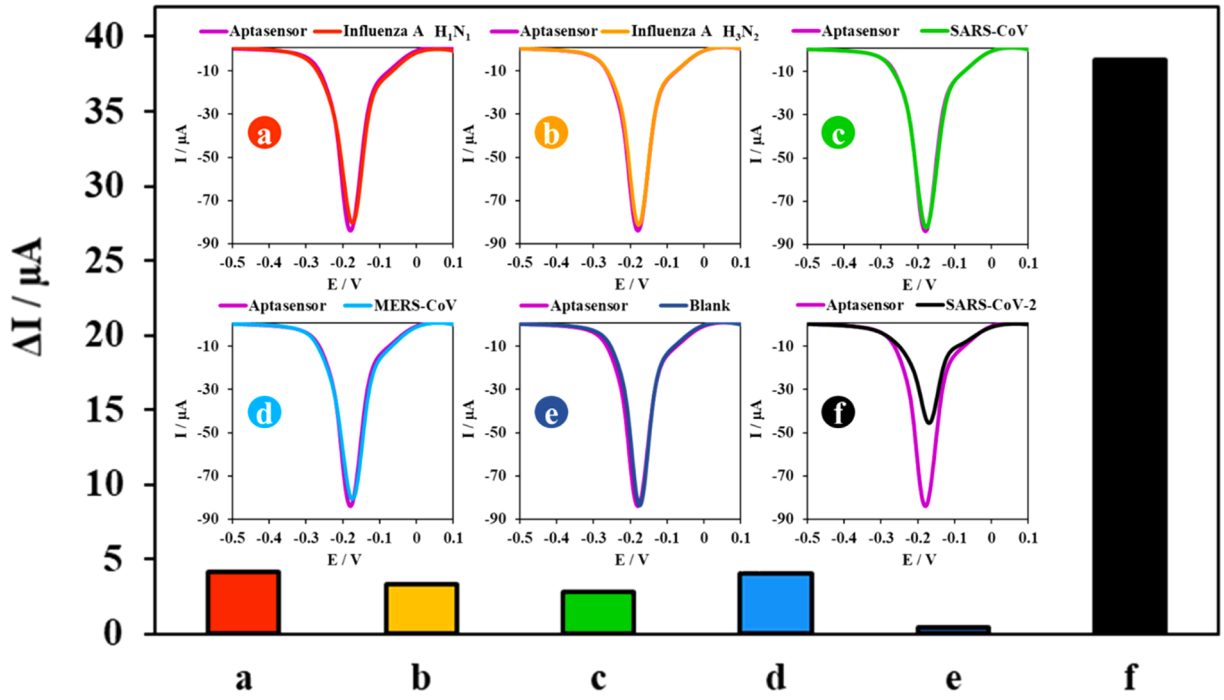

Fig. 6. (A) SWV response in PBS pH = 7.4 and histogram of then aptasensor after incubation with influenza A H_1N_1, influenza A H_3N_2, SARS-CoV, MERS-CoV and blank.

highest aptasensor response of in the minimum time, the optimum time for aptamer incubation was assessed with SARS-CoV-2 glycoprotein molecules, and, hence, the maximum answer was obtained in 15 min (Fig. S2D).

Moreover, Besides, it is worth mentioning that EIS was applied to monitor each electrode signal for further confirmation. As shown in the inset in Fig. S2, signal growth stopped after reaching the optimal values of each parameter. The results showed that the EIS signals were consistent with SWV.

3.4. SWV performance of the aptasensor for SARS-CoV-2 glycoprotein molecules determination

The SWV experiment was applied to evaluate aptasensor performance based on $Cu(OH)_2$ NRs in PBS (pH = 7.4) ranging from 0.1 to −0.5 V with the optimum conditions (Fig. 3C). By incubating different concentrations of SARS-CoV-2 spike glycoprotein on the provided aptasensor surface, the amount of $Cu(OH)_2$ NRs-associated SWV peak current decreased in proportion to the SARS-CoV-2 spike glycoprotein concentration that is due to the inhibition of $Cu(OH)_2$ NRs electron transfer by the SARS-CoV-2 spike glycoprotein-aptamer complex formation at the aptasensor surface. The calibration curve was plotted using signal (ΔI) versus SARS-CoV-2 spike glycoprotein concentration on a logarithmic scale in the range from 0.1 fg mL^{-1} to 1.2 μg mL^{-1} (Fig. 3D). The regression equation was ΔI (μA) = −5.5284 log C (fg mL^{-1}) – 17.319 (R^2 = 0.9979) and the detection limit is 0.03 ± 0.01 fg mL^{-1} (S/N = 3). The sensitivity was also 1974.43 μA mM^{-1} cm^{-2}. The provided aptasensor performance was compared with some previous reports. Table S1 showed a better detection limit and dynamic range than other reports of the provided electrobiosensor.

The good sensitivity of the provided aptasensor based on label-free approach may be attributed to use of unique $Cu(OH)_2$ NRs with high surface area and biocompatible environment structure, which provides a great surface area aimed at more loading of aptamer strings that increase the electrochemical signal as well as improves the sensitivity of the detection.

3.5. Selectivity, reproducibility, repeatability, and stability of the aptasensor

Selectivity plays a key part in the evaluation of aptasensor. Interference tests were performed to assurance that the provided aptasensor could test precisely, and its selectivity was investigated by SWV, under the same conditions, by comparing the amount of ΔI_{pc} after incubation of 500 fg mL^{-1} of target and other interactions including influenza A H_1N_1, influenza A H_3N_2, SARS-CoV and MERS-CoV. As Fig. 6 shown, a large SWV response was generated by SARS-CoV-2 spike glycoprotein incubation while no significant response was observed in the attendance of off-target species. According to the obtained results, the provided aptasensor has excellent selectivity, that can be attributed to the selectivity and affinity of aptamer strings for SARS-CoV-2 spike glycoprotein and blocking of active sites remaining by BSA and avoiding unspecific adsorption.

The robustness and accuracy of the provided aptasensor, as a significant factor, was examined by SWV with five different electrodes (reproducibility, Fig. S3A) and five successive examinations for the same electrode (repeatability, Fig. S3B). The reproducibility of the provided aptasensor was assessed via five independent electrodes provided with the same experimental situation. Similar SWV responses were observed for aptasensors to measure 5 fg mL^{-1} SARS-CoV-2 spike glycoprotein with 4.1% RSD, indicating very good aptasensor reproducibility (Fig. S3B), as well as, for five recurrent measurements of 500 fg mL^{-1} of SARS-CoV-2 spike glycoprotein, an RSD = 1.6% value was obtained, signifying that the provided aptasensor has suitable repeatability.

Additional interesting feature of this provided aptasensor was its high working stability. The aptasensor stability was measured after the incubated with SARS-CoV-2 spike glycoprotein (500 fg mL^{-1}), and storage at 4° C for 10 days. The results obtained showed that in the SWV response compared to the initial measurement only a decrease of about 2.5% was observed, that designates the excellent stability of the provided aptasensor (Fig. S3C).

Table 1
Measurement of SARS-CoV-2 spike glycoprotein in actual samples with provided aptasensor (n = 3).

Sample	Added	Measured		Rec. (%)
		Average	RSD (%)	
VTM	5 fg mL^{-1}	4.9 fg mL^{-1}	2.9	98
	40 pg mL^{-1}	38.8 pg mL^{-1}	3.6	97
	12 ng mL^{-1}	12.5 ng mL^{-1}	3.9	104
Saliva	5 fg mL^{-1}	5.1 fg mL^{-1}	2.7	102
	40 pg mL^{-1}	41.8 pg mL^{-1}	3.3	104
	12 ng mL^{-1}	11.8 ng mL^{-1}	3.8	98

Table 2
Detection of SARS-CoV-2 virus in clinical samples with provided aptasensor.

Patients	PCR test	Aptasensor test	Patients	PCR test	Aptasensor test
#1	+	+	#16	−	−
#2	+	+	#17	−	−
#3	+	+	#18	−	−
#4	+	+	#19	−	−
#5	+	+	#20	−	−
#6	+	+	#21	−	−
#7	+	+	#22	−	−
#8	+	+	#23	−	−
#9	+	+	#24	−	−
#10	+	+	#25	−	−
#11	+	+	#26	−	−
#12	+	+	#27	−	−
#13	+	+	#28	−	−
#14	+	+	#29	−	−
#15	+	+	#30	−	−

3.6. Practical application

The practical performance of the aptasensor was assessed to analysis the reliability of the method in detecting actual samples. For this aim, saliva and VTM samples were diluted 5 times by PBS and three different concentrations of SARS-CoV-2 spike glycoprotein were spiked to them. Each sample was analyzed through the aptasensor using standard addition method and SWV in the PBS under optimal conditions. The results abridged in Table 1 show the recoveries in the range of 97–104 and the RSD values are all less than 4%, which proved that the developed electrochemical aptasensor is reliable for diagnosing SARS-CoV-2 spike glycoprotein in actual samples. Moreover, the results presented that the provided aptasensor was talented to detect of SARS-CoV-2 infection as benchmarked by PCR test with 100% sensitivity (positive percent agreement) and samples of healthy individuals with 100% specificity (negative percent agreement) (Table 2). These results displayed that the provided aptasensor was talented to detect coronavirus in actual clinical samples.

4. Conclusions

In summary, a label-free and ultrasensitive electrochemical aptasensor based on direct growth $Cu(OH)_2$ NRs as sensing platform was provided. $Cu(OH)_2$ NRs by providing a high active surface can not only act as a biocompatible scaffold to anchor aptamer strings and load them further, but also as an electrochemical probe. This strategy exhibited wide dynamic range in of 0.1 fg mL^{-1} to 1.2 μg mL^{-1} and with a high sensitivity of 1974.43 μA mM^{-1} cm^{-2} and low detection limit of 0.03 ± 0.01 fg mL^{-1} of SARS-CoV-2 spike glycoprotein and led to the development of one of the most sensitive electrochemical aptasensors capable of detecting SARS-CoV-2 spike glycoprotein with ultra-trace levels in saliva and VTM samples, as well as the provided aptasensor was usable in clinical trials to detect the SARS-CoV-2 virus in real samples of sick and healthy individuals. The provided aptasensor showed advantages such as excellent selectivity, wide dynamic range, low cost, good stability, good accuracy and precision and superior sensitivity. Though the provided strategy attentive on SARS-CoV-2 detection, it could possibly and widely be used with other analysts to create sensitive and stable biosensors as a significant tool for diagnosis of other pathogens.

5. Compliance with ethical standards

All experimental protocols were approved by the Experimentation Ethics Committee of Ilam University (Code: IR.ILAM.REC.1400.013). The clinical samples were provided from a local clinical laboratory. Informed consent was obtained from all participants included in the study.

Declaration of Competing Interest

The authors declare that they have no known competing financial interests or personal relationships that could have appeared to influence the work reported in this paper.

Acknowledgment

The authors would like to thank Ilam University for supporting this research work.

Appendix A. Supplementary material

Supplementary data to this article can be found online at https://doi.org/10.1016/j.bioelechem.2022.108106.

References

[1] J.G. Manjunatha, B.E.K. Swamy, G.P. Mamatha, O. Gilbert, M.T. Shreenivas, B. S. Sherigara, Electrocatalytic response of dopamine at mannitol and Triton X-100 modified carbon paste electrode: A cyclic voltammetric study, Int. J. Electrochem. Sci. 4 (2009) 1706–1718.
[2] G.K. Jayaprakash, B.E.K. Swamy, S. Rajendrachari, S.C. Sharma, R. Flores-Moreno, Dual descriptor analysis of cetylpyridinium modified carbon paste electrodes for ascorbic acid sensing applications, J. Mol. Liq. 334 (2021), 116348.
[3] J.G. Manjunathaa, M. Deraman, N.H. Basri, I.A. Talib, Selective detection of dopamine in the presence of uric acid using polymerized phthalo blue film modified carbon paste electrode, in: Adv. Mater. Res., Trans Tech Publ, 2014, pp. 447–451.
[4] G. Tigari, J.G. Manjunatha, A surfactant enhanced novel pencil graphite and carbon nanotube composite paste material as an effective electrochemical sensor for determination of riboflavin, J. Sci.: Adv. Mater. Devices 5 (1) (2020) 56–64.
[5] N. Hareesha, J.G. Manjunatha, Elevated and rapid voltammetric sensing of riboflavin at poly (helianthin dye) blended carbon paste electrode with heterogeneous rate constant elucidation, J. Iran. Chem. Soc. 17 (6) (2020) 1507–1519.
[6] N. Hareesha, J.G. Manjunatha, Fast and enhanced electrochemical sensing of dopamine at cost-effective poly (DL-phenylalanine) based graphite electrode, J. Electroanal. Chem. 878 (2020), 114533.
[7] M. Roushani, Z. Rahmati, M. Golchin, Z. Lotfi, M. Nemati, Electrochemical immunosensor for determination of Staphylococcus aureus bacteria by IgY immobilized on glassy carbon electrode with electrodeposited gold nanoparticles, Microchim. Acta 187 (2020) 567, https://doi.org/10.1007/s00604-020-04547-6.
[8] P. Mohankumar, J. Ajayan, T. Mohanraj, R. Yasodharan, Recent developments in biosensors for healthcare and biomedical applications: A review, Measurement 167 (2021) 108293, https://doi.org/10.1016/j.measurement.2020.108293.
[9] P. Estrela, N. Bhalla, P. Jolly, N. Formisano, P. Estrela, Introduction to biosensors, Essays Biochem. 60 (1) (2016) 1–8.
[10] Z. Rahmati, M. Roushani, H. Hosseini, Hierarchical nickel hydroxide nanosheets grown on hollow nitrogen doped carbon nanoboxes as a high-performance surface substrate for alpha-fetoprotein cancer biomarkers electrochemical aptasensing, Talanta 237 (2022), 122924, https://doi.org/10.1016/j.talanta.2021.122924.
[11] X. Yu, H. Yang, X. Huang, Novel method for structure–activity relationship of aptamer sequences for human prostate cancer, ACS Omega 3 (8) (2018) 10002–10007.
[12] M. Jauset-Rubio, M.S. El-Shahawi, A.S. Bashammakh, A.O. Alyoubi, C. K. O'Sullivan, Advances in aptamers-based lateral flow assays, TrAC, Trends Anal. Chem. 97 (2017) 385–398.
[13] A. Khanmohammadi, A. Aghaie, E. Vahedi, A. Qazvini, M. Ghanei, A. Afkhami, A. Hajian, H. Bagheri, Electrochemical biosensors for the detection of lung cancer biomarkers: A review, Talanta 206 (2020) 120251, https://doi.org/10.1016/j.talanta.2019.120251.
[14] A. Dhiman, P. Kalra, V. Bansal, J.G. Bruno, T.K. Sharma, Aptamer-based point-of-care diagnostic platforms, Sens. Actuators B Chem. 246 (2017) 535–553.

[15] J. Shen, Y. Li, H. Gu, F. Xia, X. Zuo, Recent development of sandwich assay based on the nanobiotechnologies for proteins, nucleic acids, small molecules, and ions, Chem. Rev. 114 (15) (2014) 7631–7677.

[16] C. Tuerk, L. Gold, Systematic evolution of ligands by exponential enrichment: RNA ligands to bacteriophage T4 DNA polymerase, Science (80-.) 249 (1990) 505–510.

[17] H. Ye, B. Qin, Y. Sun, J. Li, Electrochemical detection of VEGF165 lung cancer marker based on Au-Pd alloy assisted aptasenor, Int. J. Electrochem. Sci. 12 (2017) 1818–1828.

[18] L. Kashefi-Kheyrabadi, M.A. Mehrgardi, E. Wiechec, A.P.F. Turner, A. Tiwari, Ultrasensitive detection of human liver hepatocellular carcinoma cells using a label-free aptasensor, Anal. Chem. 86 (10) (2014) 4956–4960.

[19] N. Hedayati, S.M. Taghdisi, R. Yazdian-Robati, A. Mansouri, K. Abnous, S. A. Mohajeri, Selection of DNA aptamers for tramadol through the systematic evolution of ligands by exponential enrichment method for fabrication of a sensitive fluorescent aptasensor based on graphene oxide, Spectrochim. Acta Part A Mol. Biomol. Spectrosc. 259 (2021), 119840.

[20] R.R. Breaker, Natural and engineered nucleic acids as tools to explore biology, Nature 432 (7019) (2004) 838–845.

[21] Y. Du, S. Dong, Nucleic acid biosensors: recent advances and perspectives, Anal. Chem. 89 (2017) 189–215.

[22] L.-S. Liu, J.-M. Kim, W.-S. Kim, Simple and reliable quartz crystal microbalance technique for determination of solubility by cooling and heating solution, Anal. Chem. 87 (6) (2015) 3329–3335.

[23] S.D. Jayasena, Aptamers: an emerging class of molecules that rival antibodies in diagnostics, Clin. Chem. 45 (1999) 1628–1650.

[24] Z. Rahmati, M. Roushani, H. Hosseini, Three-dimensional NiCo2O4 nanowires encapsulated in nitrogen-doped carbon networks as a high-performance aptamer stabilizer for impedimetric ultrasensitive detection of hepatitis C virus core antigen, Surf. Interfaces 22 (2021) 100813, https://doi.org/10.1016/j.surfin.2020.100813.

[25] E. Sánchez-Báscones, F. Parra, M.J. Lobo-Castañón, Aptamers against viruses: Selection strategies and bioanalytical applications, TrAC, Trends Anal. Chem. 143 (2021), 116349, https://doi.org/10.1016/j.trac.2021.116349.

[26] M. Citartan, Aptamers as the powerhouse of dot blot assays, Talanta 232 (2021), 122436, https://doi.org/10.1016/j.talanta.2021.122436.

[27] H. Yoo, H. Jo, S.S. Oh, Detection and beyond: challenges and advances in aptamer-based biosensors, Mater. Adv. 1 (2020) 2663–2687.

[28] M. Roushani, Z. Rahmati, S.J. Hoseini, R.H. Fath, Impedimetric ultrasensitive detection of chloramphenicol based on aptamer MIP using a glassy carbon electrode modified by 3-ampy-RGO and silver nanoparticle, Colloids Surfaces B Biointerfaces. 183 (2019), 110451.

[29] G. Evtugyn, A. Porfireva, T. Kulikova, T. Hianik, Recent Achievements in Electrochemical and Surface Plasmon Resonance Aptasensors for Mycotoxins Detection, Chemosensors. 9 (2021) 180.

[30] P. Weerathunge, R. Ramanathan, V.A. Torok, K. Hodgson, Y. Xu, R. Goodacre, B. K. Behera, V. Bansal, Ultrasensitive colorimetric detection of murine norovirus using NanoZyme aptasensor, Anal. Chem. 91 (5) (2019) 3270–3276.

[31] F. Costantini, N. Lovecchio, A. Ruggi, C. Manetti, A. Nascetti, M. Reverberi, G. de Cesare, D. Caputo, Fluorescent label-free aptasensor integrated in a lab-on-chip system for the detection of ochratoxin a in beer and wheat, ACS Appl. Bio Mater. 2 (12) (2019) 5880–5887.

[32] F. Ghorbani, H. Abbaszadeh, J.E.N. Dolatabadi, L. Aghebati-Maleki, M. Yousefi, Application of various optical and electrochemical aptasensors for detection of human prostate specific antigen: A review, Biosens. Bioelectron. 142 (2019) 111484, https://doi.org/10.1016/j.bios.2019.111484.

[33] F. Arduini, A. Amine, C. Majorani, F. Di Giorgio, D. De Felicis, F. Cataldo, D. Moscone, G. Palleschi, High performance electrochemical sensor based on modified screen-printed electrodes with cost-effective dispersion of nanostructured carbon black, Electrochem. Commun. 12 (3) (2010) 346–350.

[34] A. Abi, Z. Mohammadpour, X. Zuo, A. Safavi, Nucleic acid-based electrochemical nanobiosensors, Biosens. Bioelectron. 102 (2018) 479–489.

[35] F. Vajhadin, S. Ahadian, J. Travas-Sejdic, J. Lee, M. Mazloum-Ardakani, J. Salvador, G.E. Aninwene II, P. Bandaru, W. Sun, A. Khademhossieni, Electrochemical cytosensors for detection of breast cancer cells, Biosens. Bioelectron. 151 (2020), 111984.

[36] H. Wang, J. Sun, L. Lu, X. Yang, J. Xia, F. Zhang, Z. Wang, Competitive electrochemical aptasensor based on a cDNA-ferrocene/MXene probe for detection of breast cancer marker Mucin1, Anal. Chim. Acta 1094 (2020) 18–25, https://doi.org/10.1016/j.aca.2019.10.003.

[37] X. Huang, Y. Zhu, E. Kianfar, Nano Biosensors: Properties, applications and electrochemical techniques, J. Mater. Res. Technol. 12 (2021) 1649–1672, https://doi.org/10.1016/j.jmrt.2021.03.048.

[38] M. Negahdary, H. Heli, Applications of nanoflowers in biomedicine, Recent Pat. Nanotechnol. 12 (1) (2018) 22–33.

[39] M. Mahmoudpour, S. Ding, Z. Lyu, G. Ebrahimi, D. Du, J. Ezzati Nazhad Dolatabadi, M. Torbati, Y. Lin, Aptamer functionalized nanomaterials for biomedical applications: Recent advances and new horizons, Nano Today 39 (2021) 101177, https://doi.org/10.1016/j.nantod.2021.101177.

[40] M. Hasanzadeh, R. Sahmani, E. Solhi, A. Mokhtarzadeh, N. Shadjou, S. Mahboob, Ultrasensitive immunoassay of carcinoma antigen 125 in untreated human plasma samples using gold nanoparticles with flower like morphology: a new platform in early stage diagnosis of ovarian cancer and efficient management, Int. J. Biol. Macromol. 119 (2018) 913–925.

[41] M. Liu, R. Liu, W. Chen, Graphene wrapped Cu2O nanocubes: non-enzymatic electrochemical sensors for the detection of glucose and hydrogen peroxide with enhanced stability, Biosens. Bioelectron. 45 (2013) 206–212.

[42] C. Zhu, G. Yang, H.e. Li, D. Du, Y. Lin, Electrochemical sensors and biosensors based on nanomaterials and nanostructures, Anal. Chem. 87 (1) (2015) 230–249.

[43] A. Walcarius, S.D. Minteer, J. Wang, Y. Lin, A. Merkoçi, Nanomaterials for bio-functionalized electrodes: recent trends, J. Mater. Chem. B 1 (38) (2013) 4878, https://doi.org/10.1039/c3tb20881h.

[44] Z. Rahmati, M. Roushani, H. Hosseini, H. Choobin, Electrochemical immunosensor with Cu 2 O nanocube coating for detection of SARS-CoV-2 spike protein, Microchim. Acta 188 (2021) 1–9.

[45] F. Shahdost-fard, M. Roushani, Architecting of a biodevice based on a screen-printed carbon electrode modified with the NiONP nanolayer and aptamer in BCM-7 detection, Colloids Surfaces B Biointerfaces. 190 (2020) 110932, https://doi.org/10.1016/j.colsurfb.2020.110932.

[46] K. Ghanbari, M. Roushani, A nanohybrid probe based on double recognition of an aptamer MIP grafted onto a MWCNTs-Chit nanocomposite for sensing hepatitis C virus core antigen, Sens. Actuators B Chem. 258 (2018) 1066–1071, https://doi.org/10.1016/j.snb.2017.11.145.

[47] Y. Li, L. Deng, C. Deng, Z. Nie, M. Yang, S. Si, Simple and sensitive aptasensor based on quantum dot-coated silica nanospheres and the gold screen-printed electrode, Talanta 99 (2012) 637–642, https://doi.org/10.1016/j.talanta.2012.06.054.

[48] Y. Song, M. Xu, X. Liu, Z. Li, C. Wang, Q. Jia, Z. Zhang, M. Du, A label-free enrofloxacin electrochemical aptasensor constructed by a semiconducting CoNi-based metal–organic framework (MOF), Electrochim. Acta 368 (2021), 137609, https://doi.org/10.1016/j.electacta.2020.137609.

[49] X. Wang, F. Gao, Y. Gong, G. Liu, Y. Zhang, C. Ding, Electrochemical aptasensor based on conductive supramolecular polymer hydrogels for thrombin detection with high selectivity, Talanta 205 (2019), 120140.

[50] Z. Rahmati, M. Roushani, H. Hosseini, H. Choobin, An electrochemical immunosensor using SARS-CoV-2 spike protein-nickel hydroxide nanoparticles bio-conjugate modified SPCE for ultrasensitive detection of SARS-CoV-2 antibodies, Microchem. J. 170 (2021), 106718.

[51] G. Maduraiveeran, M. Sasidharan, W. Jin, Earth-abundant transition metal and metal oxide nanomaterials: Synthesis and electrochemical applications, Prog. Mater Sci. 106 (2019) 100574, https://doi.org/10.1016/j.pmatsci.2019.100574.

[52] H.F. Assaf, H. Salah, N. Hashem, M. Khodari, A. Toghan, Fabrication of an electrochemical sensor based on copper waste wire recycling and its application, Sens. Actuators A Phys. 331 (2021), 112962.

[53] Z. Hatami, F. Jalali, M. Amouzadeh Tabrizi, M. Shamsipur, Application of metal-organic framework as redox probe in an electrochemical aptasensor for sensitive detection of MUC1, Biosens. Bioelectron. 141 (2019), 111433, https://doi.org/10.1016/j.bios.2019.111433.

[54] R. Manafi-Yeldaghermani, S. Shahrokhian, M.H. Kahnamouei, Facile preparation of a highly sensitive non-enzymatic glucose sensor based on the composite of Cu (OH) 2 nanotubes arrays and conductive polypyrrole, Microchem. J. 169 (2021), 106636.

[55] S. Shahrokhian, E. Khaki Sanati, H. Hosseini, Advanced on-site glucose sensing platform based on a new architecture of free-standing hollow Cu (OH) 2 nanotubes decorated with CoNi-LDH nanosheets on graphite screen-printed electrode, Nanoscale 11 (26) (2019) 12655–12671.

[56] S. Shahrokhian, E. Khaki Sanati, H. Hosseini, Direct growth of metal-organic frameworks thin film arrays on glassy carbon electrode based on rapid conversion step mediated by copper clusters and hydroxide nanotubes for fabrication of a high performance non-enzymatic glucose sensing platform, Biosens. Bioelectron. 112 (2018) 100–107.

[57] D.i. Zhu, M. Yan, R. Chen, Q.i. Liu, J. Liu, J. Yu, H. Zhang, M. Zhang, P. Liu, J. Li, J. Wang, 3D Cu (OH) 2 nanowires/carbon cloth for flexible supercapacitors with outstanding cycle stability, Chem. Eng. J. 371 (2019) 348–355.

[58] P. Xu, C. Miao, J. Feng, K. Cheng, K.e. Ye, J. Yin, D. Cao, G. Wang, Z. Cai, Q. Li, A novel material NiOOH directly grown on in-situ etched Cu (OH) 2 nanowire with high performance of electrochemical energy storage, Electrochim. Acta 232 (2017) 445–455.

[59] N. Kacherovsky, L.F. Yang, H.V. Dang, E.L. Cheng, I.I. Cardle, A.C. Walls, M. McCallum, D.L. Sellers, F. DiMaio, S.J. Salipante, D. Corti, D. Veesler, S.H. Pun, Discovery and Characterization of Spike N-Terminal Domain-Binding Aptamers for Rapid SARS-CoV-2 Detection, Angew. Chem. 133 (39) (2021) 21381–21385.

[60] W. Zhang, X. Wen, S. Yang, Y. Berta, Z.L. Wang, Single-crystalline scroll-type nanotube arrays of copper hydroxide synthesized at room temperature, Adv. Mater. 15 (10) (2003) 822–825.

[61] H. Hosseini, S. Shahrokhian, Self-supported nanoporous Zn–Ni–Co/Cu selenides microball arrays for hybrid energy storage and electrocatalytic water/urea splitting, Chem. Eng. J. 375 (2019), 122090.

[62] R. Babić, M. Metikoš-Huković, A. Jukić, A study of copper passivity by electrochemical impedance spectroscopy, J. Electrochem. Soc. 148 (4) (2001) B146, https://doi.org/10.1149/1.1354608.

[63] A. Naseer, A.Y. Khan, A study of growth and breakdown of passive film on copper surface by electrochemical impedance spectroscopy, Turkish J. Chem. 33 (2009) 739–750.